Korean J. Chem. Eng., **27**(1), 76-82 (2010)
DOI: 10.2478/s11814-010-0099-5

Catalytic decomposition of nitrous oxide over Fe-BEA zeolites: Essential components of iron active sites

Mi-Young Kim*, Ki Won Lee*, Jung-Hyun Park, Chae-Ho Shin**, Jaeyoung Lee***, and Gon Seo*,†**

*School of Applied Chemical Engineering and The Research Institute for Catalysis,
Chonnam National University, Youngbong-dong 300, Gwangju 500-757, Korea
**Department of Chemical Engineering, Chungbuk National University, Cheongju, Chungbuk 361-763, Korea
***Electrochemical Reaction and Technology Laboratory (ERTL), Department of Environmental Science and Engineering,
GIST, Oryong-dong 1, Gwangju 500-712, Korea
(*Received 16 September 2009 • accepted 23 November 2009*)

Abstract−The catalytic decomposition of N_2O was investigated over Fe-BEA zeolites treated with various methods such as reduction, steaming and dissolution with potassium nitrate and nitric acid solutions in order to deduce the essential components of the active sites for the decomposition. The iron species were characterized by XPS, XANES, ESR, NO adsorption, and linear sweep voltammetry. The reduction-treated Fe-BEA zeolite with the large amounts of Fe(II) and Fe(III) species showed the highest activity. On the contrary, the dissolution treatment with the potassium nitrate solution seriously deteriorated the catalytic activity of the Fe-BEA zeolite by agglomerating iron oxide clusters and interaction between iron and potassium atoms. The catalytic roles of Fe(II)/Fe(III) species and the negative effect of potassium on the catalytic activity of the Fe-BEA zeolites were discussed.

Key words: N_2O Decomposition, Fe-BEA Zeolite, Treatment, Active Site

INTRODUCTION

The regulation of the emission of global warming gases has become an urgent issue for the preservation of the earth's environment. Although CO_2 is the most dangerous global warming gas because of its huge emissions, N_2O has a global warming potential 310-fold greater than that of CO_2 [1]. Furthermore, N_2O molecules also accelerate the dissociation of ozone. Therefore, N_2O emission from manufacturing sites for adipic acid and nitric acid is strongly regulated [1-3].

N_2O does not decompose at temperatures below 650 °C because of its high thermodynamic stability [2]. Although the addition of reductants such as ammonia, carbon monoxide and hydrocarbon considerably lowers its selective decomposition temperature to nitrogen and oxygen over various catalysts, the direct decomposition of N_2O over catalysts without any reductant dosing has been studied to reduce chemical costs and simplify the removal system [4-7].

Zeolites containing iron species have been extensively studied as efficient catalysts for direct N_2O decomposition because of their high catalytic activities [8]. However, the catalytic activity of iron-containing zeolites in N_2O decomposition varied widely according to the type of zeolite used and the method of introducing the iron species, indicating the importance of the oxidation and dispersion states of the iron species [8-12]. Iron can exist in zeolites in various states: as substituted iron atoms into the framework, as dispersed iron ions in the pore wall and on the external surface, as small clusters of iron species in the pores, and as large agglomerates of iron oxides on the external surface. Small clusters of iron species in the pores have been considered responsible for the catalytic activity in the decomposition, while the substituted iron ions in the framework and large iron oxide agglomerates on the external surface are inactive [13]. Nevertheless, the continuing ambiguity on the direct correspondence between the catalytic activity and the physico-chemical state of the iron species in their working states makes it difficult to deduce the elements of the active iron sites.

The iron cluster composed of two Fe(II) atoms connecting through an oxygen atom, known as the α-state iron cluster, effectively explains the role of the iron species in the catalytic decomposition of N_2O [14,15]. The adsorption of N_2O oxidizes the iron atoms of the α-state from +2 to +3 by adsorbing an oxygen atom and emitting a nitrogen molecule. The slow desorption of oxygen molecules determines the rate of decomposition, while the desorption mechanism of oxygen remains controversial. The small iron clusters in the micropores are suitable for the formation of α-site iron clusters. Therefore, the reduction and steaming treatment of the Fe-MFI zeolite, which has only iron atoms substituted into the framework, enhances its catalytic activity by increasing α-site iron clusters. The iron species extracted from the framework form the small clusters and work as active sites in the catalytic decomposition [9]. On the contrary, it has been suggested that other phases of the iron species are active for the catalytic decomposition of nitrous oxide [9,16-18]. The high catalytic activity exhibited even by zeolites with an iron content ultimately as low as an impurity level has made it difficult to correlate the structure of the iron species with their activity [10,11]. Furthermore, the difficulty in the characterization of iron oxide, as extensively described in the literature [10], has amplified the uncertainties in the essential components of the active sites responsible for the decomposition of N_2O.

In this study, a Fe-BEA zeolite with iron atoms as substituted

†To whom correspondence should be addressed.
E-mail: gseo@chonnam.ac.kr

into its framework was used as a catalyst in the N_2O decomposition in order to investigate the essential components of the active sites. The Fe-BEA zeolite was treated in reductive and steaming atmospheres at 500 °C and underwent dissolution treatments by the solutions of potassium nitrate and nitric acid to induce different physico-chemical states of the iron species as well as different catalytic performance. The necessary components of the active sites for Fe-BEA zeolites were deduced by correlating the characterization results of the iron species to their catalytic performance in the N_2O decomposition.

EXPERIMENTAL

1. Preparation of Catalysts

A Fe-BEA zeolite used in the N_2O decomposition was provided by Heesung Catalysts Corp. The iron atoms were substituted into the zeolite framework by synthesizing it from an iron-containing synthetic mixture.

The Fe-BEA zeolite was treated by four methods. A hydrogen and nitrogen gas mixture (Shin-Il Gas, H_2/N_2=50/50 as vol%) was used as a reductant in the reduction (RE) treatment, which was conducted at 500 °C for 4 h. In the hydrothermal (HT) treatment, the zeolites were treated with water vapor diluted in a helium flow (He/H_2O=90/10 as vol%) of 100 ml min^{-1} at 500 °C for 4 h. In the salt dissolution (SD) treatment, a 0.1 N solution of potassium nitrate (Daejung, 98%) was used to dissolve small clusters of iron species in the Fe-BEA zeolite. A 0.1 N solution of nitric acid (Aldrich, 70%) was used to remove iron species from the Fe-BEA zeolite in the acid dissolution (AD) treatment. The Fe-BEA zeolites treated with the reductant flow, steam, potassium nitrate solution and nitric acid solution were denoted by adding RE, HT, SD, AD to the ends of Fe-BEA, respectively. The original untreated Fe-BEA zeolite was itemized by adding 'orig' after its names.

2. Characterization of Catalysts

The chemical compositions of the Fe-BEA zeolites were determined by an ICP-AES (Perkin-Elmer Optima 4300 DV). The sample was dissolved with 6 ml mixture of hydrogen fluoride (Aldrich, 70%) and nitric acid (Aldrich, 99.9%) in a Teflon vessel equipped with an air-tight cover. Then the mixture was placed in an oven at 100 °C for 12 h. After removing the acid, nitric acid was added to the dissolved mixture and filled up to 8 ml.

The adsorption isotherms of nitrogen on the Fe-BEA zeolites were obtained using an automatic volumetric adsorption apparatus (Mirae SI, NanoPorosity-XQ). The Fe-BEA zeolites were evacuated at 250 °C for 3 h prior to exposure to nitrogen gas at liquid nitrogen temperature. Their surface areas were calculated using the Brunauer-Emmett-Teller (BET) equation.

The X-ray diffraction (XRD) patterns of the Fe-BEA zeolites were recorded on a high resolution X-ray diffractometer (HR-XRD, Rigaku D/MAX Ultima III) at 40 kV and 40 mA with Cu $K\alpha$ X-ray radiation (λ=0.154056 nm). The morphology and particle size of the Fe-BEA zeolites were observed using a scanning electron microscope (SEM, S-4700/Horia, Hitachi).

The X-ray absorption near-edge spectra (XANES) of the iron atoms contained in the Fe-BEA zeolites were recorded at the 3C1 beamline of the Pohang Accelerator Laboratory. The X-ray absorption of the iron atoms was measured in a fluorescence mode at the Fe *K*-edge (7,112 eV) by detuning in the range of 70-80% to eliminate higher harmonics.

The electron spin resonance (ESR) spectra of the Fe-BEA zeolites were obtained using an ESR spectrometer (JES-FA200, Jeol) at −150 °C. A catalyst sample charged in a quartz tube was irradiated with X-band (9.17 GHz) microwaves (accuracy: 1×10^{-5}) at a modulation frequency of 100 kHz. The g-factors of the ESR signals were compensated by comparison with DPPH with g=2.0036.

The IR spectra of the nitrogen monoxide (NO) adsorbed on the Fe-BEA zeolites were recorded on a Fourier-transformed infrared (FT-IR) spectrophotometer (Bio-Rad, FTS 175C). A self-supported zeolite wafer of 5 mg was evacuated at 400 °C for 1 h. After cooling to 150 °C, the catalyst wafer was exposed to NO gas (Dong-A Gas) of 30 Torr. The IR spectra were recorded after the gaseous NO was removed by evacuation.

The transmission electron micrographs (TEM) of the Fe-BEA zeolites were obtained on a Jeol JEM-2200FS electron microscope operating at 200 kV.

The chemical states of the iron and aluminum atoms dispersed on the external surface of the Fe-BEA zeolites were deduced from their X-ray photoelectron spectroscopy (XPS) spectra recorded on a VG MultiLab 2000 with non-monochromatic Mg $K\alpha$ radiation (1,253.6 eV) at a pressure of 10^{-9} Torr. The binding energies of the elements were referenced to the C1s peak at 285.0 eV.

A potentiostat/galvanostat (Autolab, PGSTAT30) was used for linear sweep voltammetry (LSV) in a three-electrode voltammetric system consisted of a glassy carbon (GC) working electrode of 3 mm in diameter, a platinum counter electrode, and a Ag/AgCl reference electrode. The GC electrode was polished on alumina powder with water. The mixed solutions of Fe-BEA zeolites were prepared by adding 5 mg zeolite and 2 mg nafion solution (Aldrich, 5 wt%). The 2 μl of the Fe-BEA zeolite solution was dropped on the GC electrode, and then the electrode was kept at 40 °C for 10 min. LSV experiments were carried out from 0.9 to - 0.25 V in 1 M HCl with a scan rate of 5 mVs^{-1}.

3. Catalytic Decomposition of N_2O

The catalytic decomposition of N_2O was conducted under atmospheric pressure in a continuous-flow apparatus with a fixed-bed quartz reactor containing 0.1 g zeolite catalyst. Prior to obtain the steady state conversions, temperature programmed decomposition of N_2O were carried out under flowing 200 cm^3/min (Dong-A gas, 5,000 ppm N_2O in He balance) from 250 to 600 °C with a heating rate 2 °C/min and then maintained at the final temperature for 1 h. After cooling to 250 °C, the decomposition of N_2O was performed at a desired temperature at the steady state conversion from 250 to 550 °C by an interval of 50 °C. The product stream was analyzed using a N_2O infrared gas analyzer (Teledyne Analytical Instruments, Model 7600). Conversion was defined as the percentage amount of N_2O converted to N_2 and O_2 per the amount of N_2O in the feed.

RESULTS AND DISCUSSIONS

1. Physico-chemical Properties of Fe-BEA Zeolites

The RE, HT, SD and AD treatments of the Fe-BEA-orig zeolite cause some changes in its composition, crystallinity, morphology and pore structure. Table 1 lists the chemical compositions and surface areas of the Fe-BEA zeolites treated with various methods.

Table 1. Physico-chemical properties of Fe-BEA zeolites

Catalyst	Si/Al ratio	Composition (wt%)[b]		S_{BET} (m^2/g)
		Fe	K	
Fe-BEA-orig	15-20[a]	1.0	-	567
Fe-BEA-RE	-	0.9	-	609
Fe-BEA-HT	-	0.9	-	530
Fe-BEA-SD	-	0.8	2.0	493
Fe-BEA-AD	-	0.3	-	589

[a]Information from the manufacturing company
[b]Measured by ICP-AES

The iron contents of Fe-BEA-RE, Fe-BEA-HT and Fe-BEA-SD were 0.8-0.9 wt%, indicating that these treatments did not cause any significant removals of iron species. However, the AD treatment lowered the iron content of Fe-BEA-AD to 0.3 wt%. Since the nitric acid solution dissolved and removed effectively iron species, the iron content was largely reduced by the AD treatment.

The Fe-BEA zeolites still maintained their XRD patterns and particle morphologies even after the treatments, regardless of the treatment methods, indicating the high stability of the zeolite framework and macroscopic shape. Nevertheless, the HT and SD treatments lowered the surface area of the Fe-BEA zeolite to 530 and 493 m^2/g, respectively. The other treatments such as RE and AD induced no significant changes in the surface area. Since the HT treatment usually removes aluminum and iron atoms of Fe-zeolites from their framework [19], a partial destruction of micropores lowers their surface areas. The high content of potassium of Fe-BEA-SD, 2 wt%, confirmed the presence of salts in the zeolite pores and their blockage of the pores resulted in a lowered surface area.

Fe *K*-edge XANES spectra provide information on the coordination state of iron species in terms of pre-edge peak and edge energy, because the conversion of the coordination state of iron species from tetrahedral to octahedral decreases the intensity of the pre-edge peak and lowers the edge energy [20,21]. Fig. 1 shows XANES spectra of iron species in the Fe-BEA zeolites. Fe-BEA-orig and Fe-BEA-SD showed definite pre-edge peak, while Fe-BEA-HT slightly decreased peak. However, the pre-edge peak of Fe-BEA-RE was negligible, indicating the definite extraction of tetrahedrally coordinated iron atoms from the framework and the formation of oxide clusters with octahedral coordination in pores. The slight increase in the pre-edge peak of Fe-BEA-SD showed the maintenance of the tetrahedral coordination of iron species during the SD treatment. The RE and HT treatments caused the extraction of iron species from the framework and the formation of oxide clusters with octahedral coordination. However, the SD treatment did not cause the change in the coordination state of iron. The low content of iron species in Fe-BEA-AD, 0.3 wt%, did not provide an appreciable pre-edge peak.

The edge energy of Fe *K*-edge determined from the XANES spectra (Fig. 1) of the Fe-BEA zeolites also confirmed the reduction of iron species with the HT and RE treatments. The edge energies of Fe_2O_3, Fe_3O_4 and FeO were 7,128, 7,124 and 7,119 eV, respectively, and the iron species with low oxidation states have low edge energies [22]. The edge energy of the Fe-BEA zeolites decreased following the order of Fe-BEA-orig (7,127 eV)>-SD (7,126 eV)>-HT (7,124 eV)>-RE (7,121 eV). Most of iron species in Fe-BEA-orig and -SD existed as Fe(III) species, but the amount of Fe(II) species increased with the HT and RE treatments. The slightly high pre-edge energy of Fe-BEA-RE, 7,121 eV, indicated that iron species were presented as the mixed state of Fe(II)/Fe(III) species.

Fe(III) species usually show ESR signals with different g-values

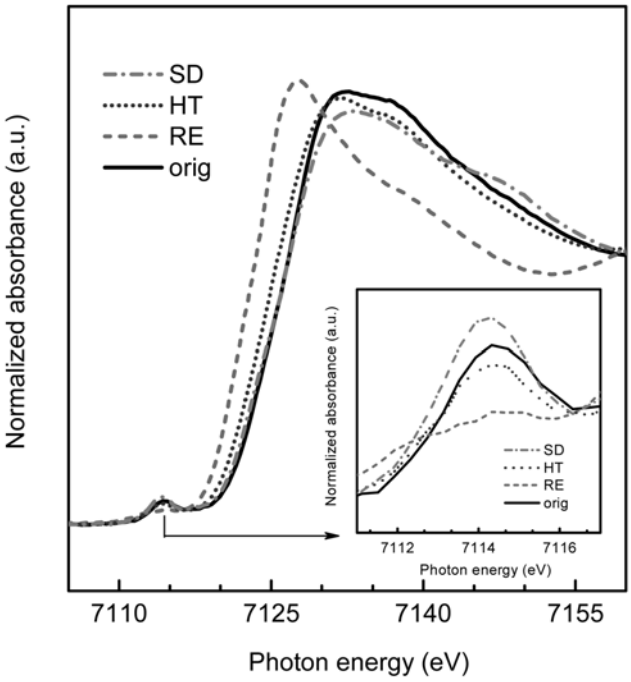

Fig. 1. Fe *K*-edge XANES spectra of Fe-BEA zeolites. The inserted figure donates enlarged peaks of the pre-edge.

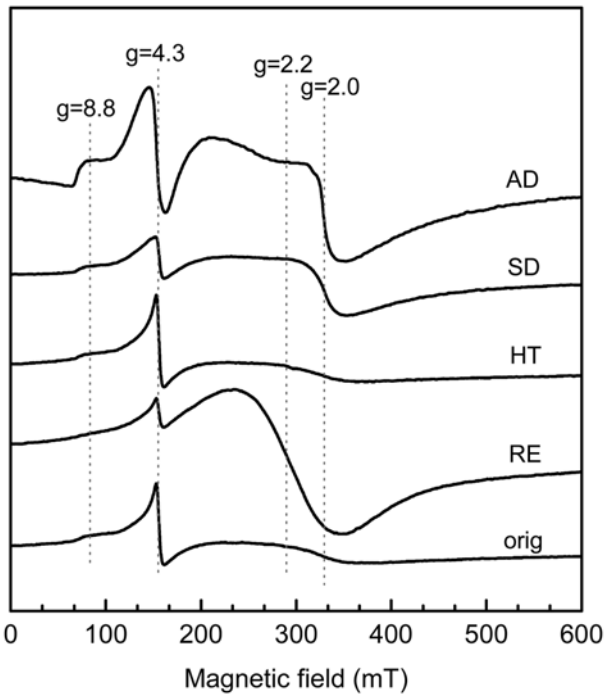

Fig. 2. ESR spectra of Fe-BEA zeolites.

according to their chemical environment [17,23-25]. Fig. 2 shows ESR spectra of the Fe-BEA zeolites treated with various methods. Four different signals were generally observed: a sharp signal with g=2.0, a broad signal with g=2.2, a very sharp signal with g=4.3 and a broad signal with g=8.8. The first signal was attributed to iron oxide clusters either isolated or within oligomerized Fe_xO_y and the second one to iron oxide clusters with Fe(III) neighbors. The small iron oxide clusters of Fe_2O_3 and iron atoms substituted to zeolite framework showed their ESR signals at g=4.3 and the agglomerated iron oxide with a pentahedral coordination at g=8.8. Fe-BEA-orig showed a sharp, intense signal with g=4.3, and thereby most of the iron species was located as framework elements. The ESR spectrum of Fe-BEA-HT was very similar to that of Fe-BEA-orig. On the contrary, the ESR signal at g=4.3 considerably decreased accompanying with the increase of the signal at g=2.2 due to the RE treatment, indicating that iron species substituted in the framework were extracted and formed iron oxide clusters in the cavities of the BEA zeolite. The increases in the signal at g=2.0 with the SD and AD treatments were also attributed to the formation of octahedrally coordinated iron oxide agglomerates. However, the higher ESR signal of Fe-BEA-AD than Fe-BEA-SD strongly pointed out that most iron species in the former was existed as isolated Fe(III) species, even though its iron content was small compared to the latter. The small ESR signal of the latter stated that iron species formed large agglomerates which were ESR inactive.

The adsorption of NO on iron species generates various absorption bands in IR spectra according to their chemical states [26,27]. Fig. 3 shows the IR spectra of NO adsorbed on the Fe-BEA zeolites. Fe-BEA-orig exhibited small bands around 1,720 and 1,870 cm^{-1} with NO adsorption. The band around 1,870 cm^{-1} was extremely intense on Fe-BEA-RE, while that on Fe-BEA-HT was slightly higher than that on Fe-BEA-orig. The Fe-BEA-SD and Fe-BEA-AD zeolites treated with the KNO_3 and HNO_3 solutions did not show any absorption around 1,870 cm^{-1}. Although the absorption band at 1,720 cm^{-1} varied with the treatment, the changes were too small to

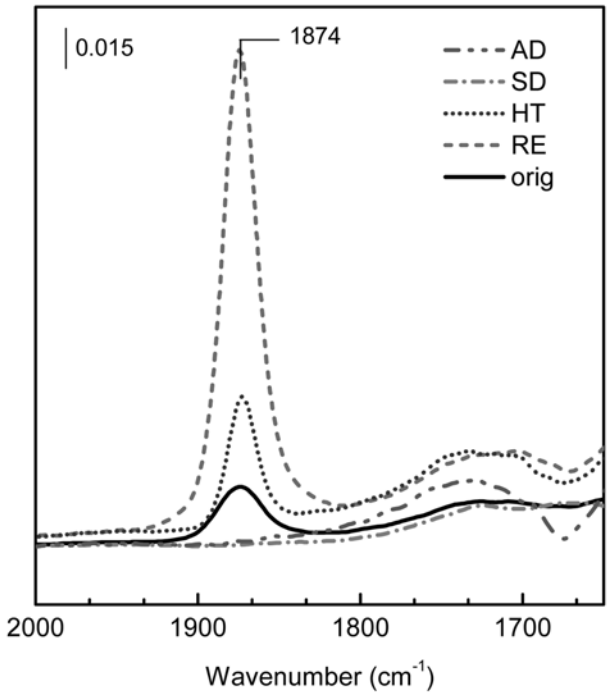

Fig. 3. Differential FT-IR spectra of NO adsorbed on Fe-BEA zeolites. The catalysts were evacuated at 400 °C for 1 h before exposing to nitrogen monoxide of 30 Torr at 150 °C.

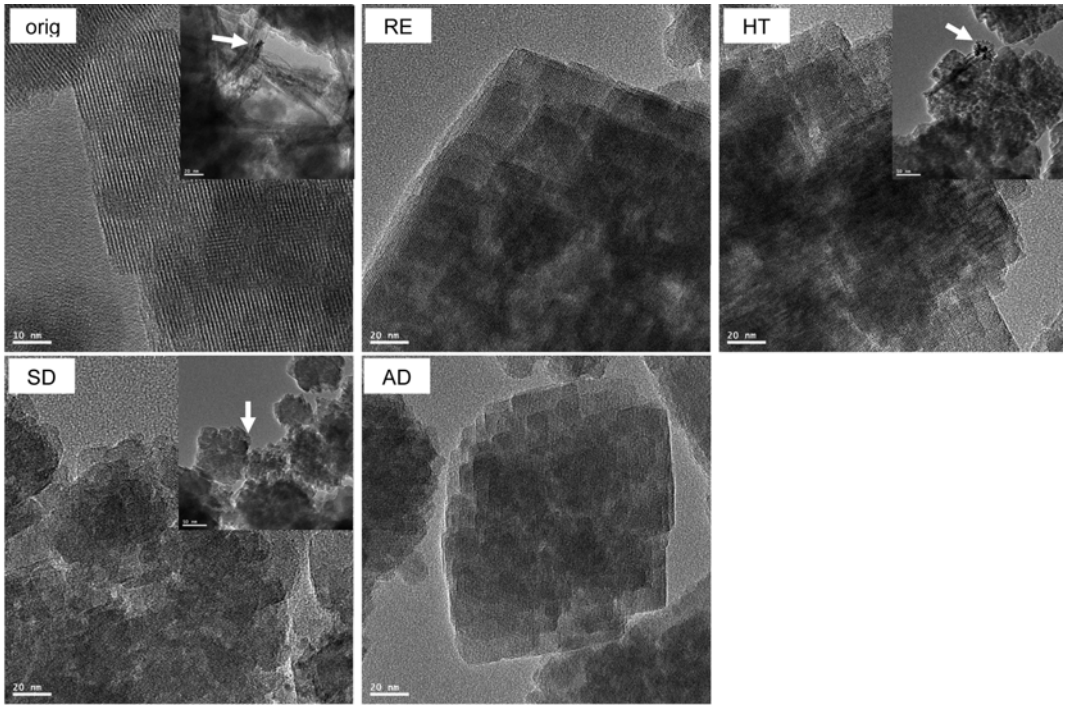

Fig. 4. TEM photos of Fe-BEA zeolites.

discuss quantitatively in relation to the chemical state of iron species.

Although controversy continues over the chemical nature of the band at 1,870 cm^{-1}, the assignment of the band to NO adsorbed on Fe(II) oxide clusters located in the large cavities of BEA zeolites has become more plausible [26]. Therefore, the appearance of the intense band at 1,870 cm^{-1} on Fe-BEA-RE with the adsorption of NO suggested the considerable increase of Fe(II) species at the RE treatment. The HT treatment also induced the formation of Fe(II) species, but the amount was not much. The Fe-BEA-SD and Fe-BEA-AD zeolites did not have the Fe(II) species accessible to NO molecules, even though both zeolites still contained iron species after the SD and AD treatments (Table 1). The KNO_3 and HNO_3 solutions dissolved the small clusters of iron species and resulted in the loss of the Fe(II) species available as the adsorption sites of NO.

TEM examination of the Fe-BEA zeolites is useful to confirm the dispersion of iron species. Fig. 4 shows their TEM photos. Well-ordered BEA zeolite lattice was observed on Fe-BEA-orig. Agglomerates of iron oxide within raging 5-10 nm were very rare, indicating that most of iron species was highly dispersed in the zeolite. This observation was good in accord with the high ESR signal at g=4.3, representing the substitution of iron species into the framework. The identification of iron oxide agglomerates on Fe-BEA-RE and Fe-BEA-AD was unsuccessful, and they showed only well-ordered lattice. On the contrary, small agglomerates of iron oxide were observed on Fe-BEA-HT and Fe-BEA-SD, even though their numbers were very small. The HT treatment extracted iron species from the framework and formed iron oxide agglomerates. The KNO_3 solution dissolved iron species, but some of them remained in zeolite pores by forming the agglomerates of iron salts. At the AD treatment the dissolved iron species were removed, and thereby iron oxide agglomerates were not observed. The reductive atmosphere of the RE treatment inhibited the formation of iron oxide agglomerates, maintaining the high dispersion of iron species.

The XPS signals of the Fe-BEA zeolites were very weak as shown in Fig. 5, indicating that most of iron species was located in zeolite pores not on the external surface. XPS peaks of Fe $2p_{3/2}$ were observed at 712.4 eV on Fe-BEA-orig. Fe-BEA-RE and Fe-BEA-HT, while that was observed at 711.4 eV on Fe-BEA-SD. Fe-BEA-AD did not show any appreciable peak relative to iron species because of its considerably low iron content. Fe $2p_{3/2}$ peak of iron oxides (Fe_2O_3) dispersed on zeolites was observed at 711.6-712.3 eV due to the strong interaction between iron species and zeolite surface [28]. Therefore, the XPS peaks of iron species at 712.4 eV indicated the presence of Fe(III) species on the external surface of the Fe-BEA zeolite. However, the low binding energy (711.4 eV) of iron species in Fe-BEA-SD reflected the increase in the electron density of iron atoms due to the interaction with potassium atoms. The low binding energy (75.1 eV) of aluminum atoms in Fe-BEA-SD compared to those (75.7 eV) of other Fe-BEA zeolites supported the explanation.

Electro-reduction of iron species in zeolites causes several responses in LSV according to their physico-chemical states [19]. The large particles of iron oxide usually require high voltage for their reduction, while the small clusters of iron oxide in zeolite pores show their reduction response at low voltage. The reduction of isolated iron oxide located on the external surface occurs around +0.3 V and that of small iron oxide clusters around +0.4 V. Fig. 6 shows linear sweep voltammograms of the GC electrodes modified with the Fe-BEA zeolites. GC electrode modified with Nafion only did not show any current-voltage profile, but that modified with Fe-BEA-orig exhibited a small peak at +0.3 V. The RE and HT treatments increased the cathodic current peaks, while the SD treatment caused a significant decrease of the current peak. No response was observed on Fe-BEA-AD. The high responses of Fe-BEA-RE at +0.4 V and Fe-BEA-HT at +0.3 V clearly showed the increase of very small Fe(III) species after the RE and HT treatments. The iron species extracted from the framework formed many isolated iron oxide clusters. On the contrary, the SD treatment induced the formation of the agglomerates of iron species, resulting in a significant decrease of the cathodic current peak. The negligible small peak of Fe-BEA-AD definitely exhibited the significant removal of iron species at the AD treatment.

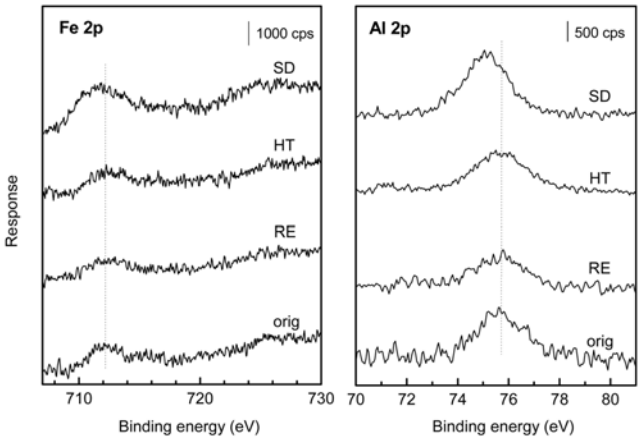

Fig. 5. XPS spectra of the Fe 2p and Al 2p peaks of Fe-BEA zeolites.

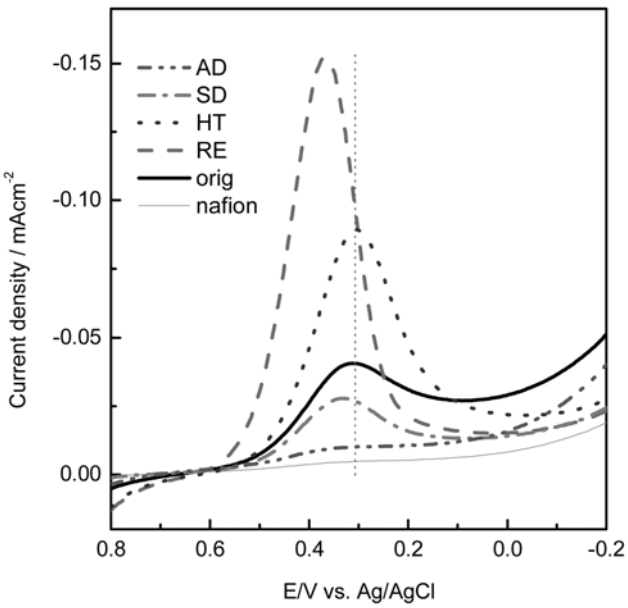

Fig. 6. Linear sweep voltammograms of grassy carbon electrodes modified by Fe-BEA zeolites in 1.0 M HCl aqueous solution.

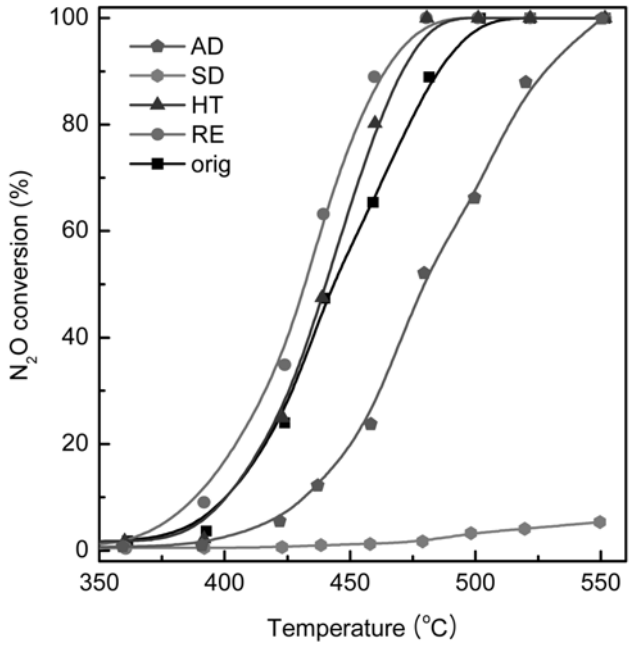

Fig. 7. Conversion profiles of N_2O over Fe-BEA zeolites. N_2O decomposition was conducted isothermally for 20 min at each temperature step.

2. Catalytic Activities of Fe-BEA Zeolites

The catalytic activity of Fe-zeolites in the N_2O decomposition considerably varied with the treatment methods [9,24,25]. Fig. 7 shows the conversion profiles of N_2O over the Fe-BEA zeolites. The RE and HT treatments shifted the conversion profiles to left by enhancing the catalytic activity, while the SD and AD treatments lowered. Especially, Fe-BEA-SD was totally inactive in the examined temperature range. The iron contents of the Fe-BEA zeolites did not considerably varied with the treatments, and maintained at the range of 0.7-0.9 wt%, except Fe-BEA-AD. On the contrary, their catalytic activities considerably varied with the treatments. This meant that the state of iron species rather than their content was more important in determining the catalytic activity.

Several researchers reported the improvement of the catalytic activity of Fe-zeolite by the RE and HT treatments [19,29]. Since the iron species substituted into the framework or agglomerated to large iron oxide particles were inactive, the treatments that extracted iron species from the framework and formed small iron oxide clusters enhanced the catalytic activity. Since the adsorption of N_2O on Fe(II) species is the first step of the N_2O decomposition [13], the RE treatment can improve the catalytic activity of Fe-zeolites by increasing the amount of Fe(II) species. Exposed iron atoms of small oxide clusters were easily reduced and produced Fe(II) species which were active in the N_2O decomposition.

The RE and HT treatments definitely achieved the enhancement of the Fe-BEA zeolite activity as mentioned above. In addition to the formation of Fe(II) species, the enhanced catalytic activity of Fe-BEA-RE was attributed to the change in the coordination state of iron species. Since the iron atoms substituted into the framework had tetrahedral coordination, the presence of octahedral iron species revealed the extraction of iron species from the framework and the formation of iron oxide clusters. The decrease in the ESR signal of g=4.3 also indicated the extraction of iron species at the RE treatment. The increase in the absorption band of NO at 1,870 cm^{-1} exhibited the abundance of Fe(II) species. Therefore, the RE treatment increased isolated Fe(II) species and achieved a high catalytic activity of Fe-BEA-RE in the N_2O decomposition.

Nevertheless, the active catalysts for the N_2O decomposition such as Fe-BEA-RE, Fe-BEA-HT and Fe-BEA-orig commonly showed high ESR signal of iron species indicating the presence of Fe(III) species. This meant that Fe(III) species as well as Fe(II) species were also necessary as an essential component of the active sites for N_2O decomposition. Fe-BEA-RE, the most active catalyst among the Fe-BEA zeolites, exhibited a large reduction signal in LSV results (Fig. 6). Its large reduction peak at +0.3 V strongly demonstrated the presence of small iron oxide clusters containing Fe(III) species. Since Fe-BEA-RE had a plenty of Fe(II) as mentioned before, the co-presence of Fe(II) and Fe(III) species was essential for the active sites with high catalytic activity in the N_2O decomposition.

Many papers reporting the N_2O decomposition suggested the structure and oxidation state of active iron species based on the changes in their physico-chemical state induced the improvement of the catalytic activity observed [19,24,25,29]. The extraction of iron species from the framework, their movement to specific sites and the reduction to Fe(II) state were typical examples caused the improvement. However, the essentially required amount of iron species in the Fe-zeolites for the N_2O decomposition was very small, and thereby the impurity level of iron species was enough for their high activity [9]. Therefore, It is very dangerous to correlate the changes in the physico-chemical state of iron species to their activity in Fe-zeolites with high iron contents. We introduced the SD and AD treatments to lower the catalytic activity in order to deduce the indispensably required state of iron species causing high activity in the N_2O decomposition.

The dilute nitric acid solution lowered the content of iron species to 0.3 wt% by dissolving and removing them. However, the Fe-BEA-AD zeolite with a low iron content maintained its catalytic activity, even though its activity was definitely low compared to Fe-BEA-orig. It's extremely low iron content hindered the examination of its physico-chemical states by using XANES, XPS, and LSV techniques providing the information on active iron species. On the other hand, the Fe-BEA-SD zeolite was completely inactive in N_2O decomposition even at high temperature range, while its iron content was sufficiently higher (0.7 wt%) than that of Fe-BEA-AD (0.3 wt%). The considerable decrease of BET surface area and the observation of iron oxide particles on the TEM photo indicated that the SD treatment removed partly iron species but most of them was remained in the zeolite pores. The small ESR signal of Fe-BEA-SD also represented the reduction of isolated Fe(III) species. The negligible absorption band of NO at 1,870 cm^{-1} also reflected the low content of Fe(II) species. However, these observations were not sufficient to explain the extremely low catalytic activity of Fe-BEA-SD.

The most significant difference of iron species in Fe-BEA SD contained 2 wt% potassium from other Fe-BEA zeolites was the shift of the binding energies of iron and aluminum atoms to lower energies. The binding energies of Fe 2p and Al 2p peaks on Fe-BEA-SD were low by about 0.5 eV compared to those on other Fe-BEA zeolites. The presence of potassium near iron and aluminum atoms

caused the increasing of their electron densities, and thereby their XPS peaks shifted to lower binding energies. The iron species dispersed in acidic zeolites usually showed higher activity than those dispersed in neutral zeolites [30]. Therefore, the partial neutralization of acidic properties of iron species by co-presence of potassium might deteriorate their catalytic activity in the N_2O decomposition. Although the catalytic role of acidic property to the N_2O decomposition was not certain yet, it was evident that the increase in the electron density of iron species was harmful for its catalytic activity.

CONCLUTIONS

The treatments of the Fe-BEA-orig zeolite with various methods such as RE, HT, AD and SD caused considerable changes in its catalytic activity in the N_2O decomposition. The RE-treated zeolite showed the highest activity, while the SD-treated one was completely inactive. The extraction of iron species from the zeolite framework and the formation of small iron oxide clusters enriched with Fe(II) species in the RE treatment enhanced the catalytic activity. The formation of agglomerates in zeolite pores and the interaction between potassium and iron species in the SD treatment was responsible for the extremely low catalytic activity. The very small iron oxide clusters with Fe(II)/Fe(III) species formed in zeolite pores were suggested to the active sites for the decomposition of N_2O.

ACKNOWLEDGEMENTS

This study was financially supported by Chonnam National University, 2007. We acknowledge the Pohang Accelerator Laboratory (PAL) for the XAS measurement and Heesung Catalysts Corporation for the supply of the Fe-BEA zeolite.

REFERENCES

1. J. Peréz-Ramírez, *Appl. Catal. B*, **70**, 31 (2007).
2. F. Kapteijn, J. Rodriguez-Mirasol and J. A. Moulijn, *Appl. Catal. B*, **9**, 25 (1996).
3. G. Centi, S. Perathoner, F. Vazzana, M. Marella, M. Tomaselli and M. Mantegazza, *Adv. Environ. Res.*, **4,** 325 (2000).
4. A. Ates, *Appl. Catal. B*, **76**, 282 (2007).
5. A. Guzmán-Vargas, G. Delahay and B. Coq, *Appl. Catal. B*, **42**, 369 (2003).
6. V. Boissel, S. Tahir and C. A. Koh, *Appl. Catal. B*, **64**, 234 (2006).
7. E. V. Kondratenko and J. Peréz-Ramírez, *Appl. Catal. B*, **64**, 35 (2006).
8. K. Jíša, J. Nováková, M. Schwarze, A. Vondrová, S. Sklenák and Z. Sobalik, *J. Catal.*, **262**, 27 (2009).
9. P. K. Roy, R. Prins and G. D. Pirngruber, *Appl. Catal. B*, **80**, 226 (2008).
10. S. Dzwigaj, J. Janas, W. Rojek, L. Stievano, F. E. Wagner, F. Averseng and M. Che, *Appl. Catal. B*, **86**, 45 (2009).
11. A. H. Øygarden and J. Peréz-Ramírez, *Appl. Catal. B*, **65**, 163 (2006).
12. J. Peréz-Ramírez, J. C. Groen, A. Brückner, M. S. Kumar, U. Bentrup, M. N. Debbagh and L. A. Villaescusa, *J. Catal.*, **232**, 318 (2005).
13. A. Zecchina, M. Rivallan, G. Berlier, C. Lamberti and G. Ricchiardi, *Phys. Chem. Chem. Phys.*, **9**, 3483 (2007).
14. K. A. Dubkov, N. S. Ovanesyan, A. A. Shteinman, E. V. Starokon and G. I. Panov, *J. Catal.*, **207**, 341 (2002).
15. E. Berrier, O. Ovsitser, E. V. Kondratenko, M. Schwidder, W. Grünert and A. Brückner, *J. Catal.*, **249**, 67 (2007).
16. D. Kaucký, Z. Sobalík, M. Schwarze, A. Vondrová and B. Wichterlová, *J. Catal.*, **238**, 293 (2006).
17. E. J. M. Hensen, Q. Zhu, R. A. J. Janssen, P. C. M. M. Magusin, P. J. Kooyman and R. A. van Santen, *J. Catal.*, **233**, 123 (2005).
18. G. Centi, S. Perathoner, R. Arrigo, G. Giordano, A. Katovic and V. Pedulà, *Appl. Catal. A*, **307**, 30 (2006).
19. J. Pérez-Ramírez, F. Kapteijn, J. C. Groen, A. Doménech, G. Mul and J. A. Moulijn, *J. Catal.*, **214**, 33 (2003).
20. G. Sankar, N. R. Shiju, I. D. Watts, S. Nikitenko and W. Bars, *Res. Chem. Intermed.*, **34**(5-7), 649 (2008).
21. S. H. Choi, B. R. Wood, J. A. Ryder and A. T. Bell, *J. Phys. Chem. B*, **107**, 11843 (2003).
22. J. S. Choi, H. K. Youn, B. H. Kwak, Q. Wang, K. S. Yang and J. S. Chung, *Appl. Catal. B*, **91**, 210 (2009).
23. M. Schwidder, M. S. Kumar, K. Klementiev, M. M. Pohl, A. Srückner and W. Grünert, *J. Catal.*, **231**, 314 (2005).
24. J. Peréz-Ramírez, M. S. Kumar and A. Brückner, *J. Catal.*, **223**, 13 (2004).
25. M. S. Kumar, M. Schwidder, W. Grünert, U. Bentrup and A. Brückner, *J. Catal.*, **239**, 173 (2006).
26. I. Yuranov, D. A. Bulushev, A. Renken and L. Kiwi-Minsker, *Appl. Catal. A*, **319**, 128 (2007).
27. T. Chaki, M. Arai, T. Ebina and M. Shimokawabe, *J. Catal.*, **218**, 220 (2003).
28. L. Čapek, V. Kreibich, J. Dědeček, T. Grygar, B. Wichterlová, Z. Sobalík, J. A. Martens, R. Brosius and V. Tokarová, *Microporous Mesoporous Mat.*, **80**, 279 (2005).
29. J. F. Jia, B. Wen and W. M. H. Sachtler, *J. Catal.*, **210**, 453 (2002).
30. M. Rivallan, G. Ricchiardi, S. Bordiga and A. Zecchina, *J. Catal.*, **264**, 104 (2009).